JOURNAL OF MATERIALS SCIENCE 17 (1982) 2384–2390

Transmission electron microscopy on nickel oxide single crystals deformed at room temperature

S. MARUYAMA*, A. GERVAIS†, J. PHILIBERT
Laboratoire de Physique des Matériaux, CNRS, 1, Place A. Briand, 92190 Meudon, France

Transmission electron microscopy was performed on nickel oxide single crystals deformed under compression along the [0 0 1] direction, at room temperature. Foils for observation were obtained by mechanical thinning followed by ion beam thinning. The glide system and the Burgers vectors of dislocations were found to be the same as those of MgO and NaCl. For the origin of high rate work hardening, the intersection of glissile dislocations with other inactive dislocations followed by dipole formation, and edge dipole formation which serves as a strong barrier against active slip dislocations, were confirmed. The second stage of work hardening begins with the operation of an oblique second system.

1. Introduction

Plastic deformation of nickel oxide single crystals has been studied in our laboratory for several years [1–4]. The study was mainly confined to that of constant strain rate compression, and of the determination of glide systems. In the present study, some preliminary transmission electron microscopy (TEM) observations were performed in order to elucidate the elementary process of deformation, and to identify the rate controlling mechanism of plastic flow, comparing results with the much investigated magnesium oxide and rock salt which have the same crystal structure.

2. Experimental procedure

Single crystals of nickel oxide, grown by a zone-melted technique in an arc image furnace [5], were cleaved, sawn and mechanically polished to about 2.5 mm × 2.5 mm × 6 mm in size, with their surface parallel to {1 0 0} planes. They were then annealed at 1200° C for about 100 h in air. A spectroscopic analysis of the crystal gave 10 ppm of Mg and 15 ppm of Si as impurities.

The specimens were deformed in compression along the long [0 0 1] direction, with a strain rate of the order of 6×10^{-5} sec^{-1}, by as much as three per cent, at room temperature, using an Instron universal testing machine.

For electron microscopic observation, the crystals were cut in slices normal to the compression axis, and were mechanically polished to about 150 μm in thickness. The thinning of the foil was achieved by ion beams. The glancing angle of the attack was set to 30° until the foil became transparent, and was diminished to 10° afterwards, in order to avoid surface relief due to ion bombardment. As soon as a small hole was found in the centre, the bombardment was stopped, and the foil was glued to a single hole grid, using silver paste, to avoid any possible deformation during handling.

As was already noticed in MgO [6, 7], the dislocation configuration in thinner regions is different from that in thicker regions. That is, the dislocations are mostly inclined in the foil, and dislocations parallel to the surface are seldom

*On leave of absence from the Department of Natural Science, Osaka Women's University, Daisen-cho, Sakai City, Osaka 590.
†Present address: Laboratoire minéralogie cristallographie, Université Paris 6, 4 Place Jussieu, Paris.

 0022–2461/82/082384–07$03.34/0

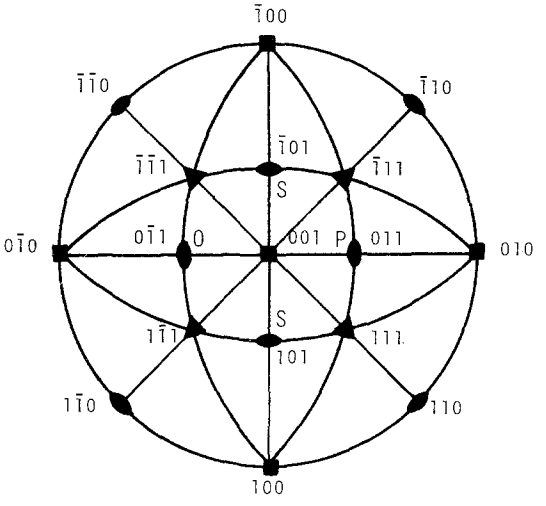

Figure 1 Nomenclature of the glide elements in NiO. P and O denote primary and orthogonal slip planes, while S denotes oblique slip planes.

found, as opposed to the case for the thicker regions. This is due to the necessary decrease in density of the dislocations parallel to the surface, partly by thinning, and partly by mirror forces acting on them. The present observation was therefore limited to regions as thick as 300 nm, in a good transition condition ($s > 0$, where s denotes the deviation parameter from the Bragg condition in reciprocal space, and is positive if the diffraction angle is larger than the Braff angle, using a 100 kV electron microscope. The direct magnification of images was in most cases kept × 33 000 for simplicity.

3. Results

3.1. Glide elements

The nomenclature used to describe the glide elements is given in Fig. 1. There is only one ⟨1 1 0⟩ slip direction in each {1 1 0} slip plane, as in the ordinary case for the NaCl type structure. In the present experiment, there are six {1 1 0} slip planes, of which four should be equally operative (two are inactive). At the beginning of the deformation, only two orthogonal slip systems, denoted by P and O in Fig. 1, were macroscopically active. The oblique system S began to operate only after 1 or 2% strain, and the rate of work hardening increased after that. This is probably due to dislocation interactions and will be treated in Section 3.2.3.

3.2. Origin of work hardening

The NiO crystals exhibit a considerable work hardening rate; 7.0×10^2 and 1.5×10^3 MN m^{-2} for the two stages at room temperature, which are

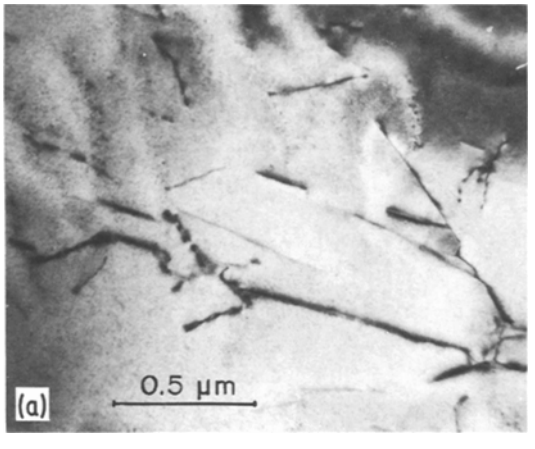

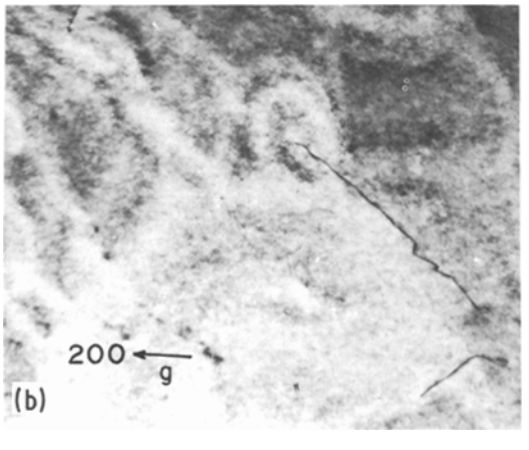

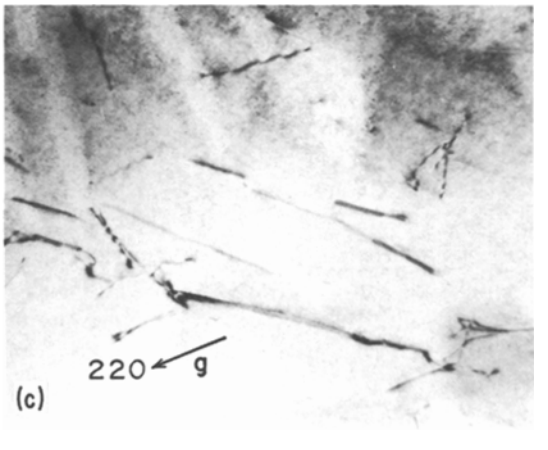

Figure 2 Intersection of primary dislocations with inactive dislocations. (a) Whole set of dislocations is revealed using multiple reflections. (b) Only the inactive dislocations are seen. Note the cusps formed in the crossed dislocation. (c) Only the primary slip dislocations are seen. They form dipoles at the cusps after surrounding the crossed dislocation.

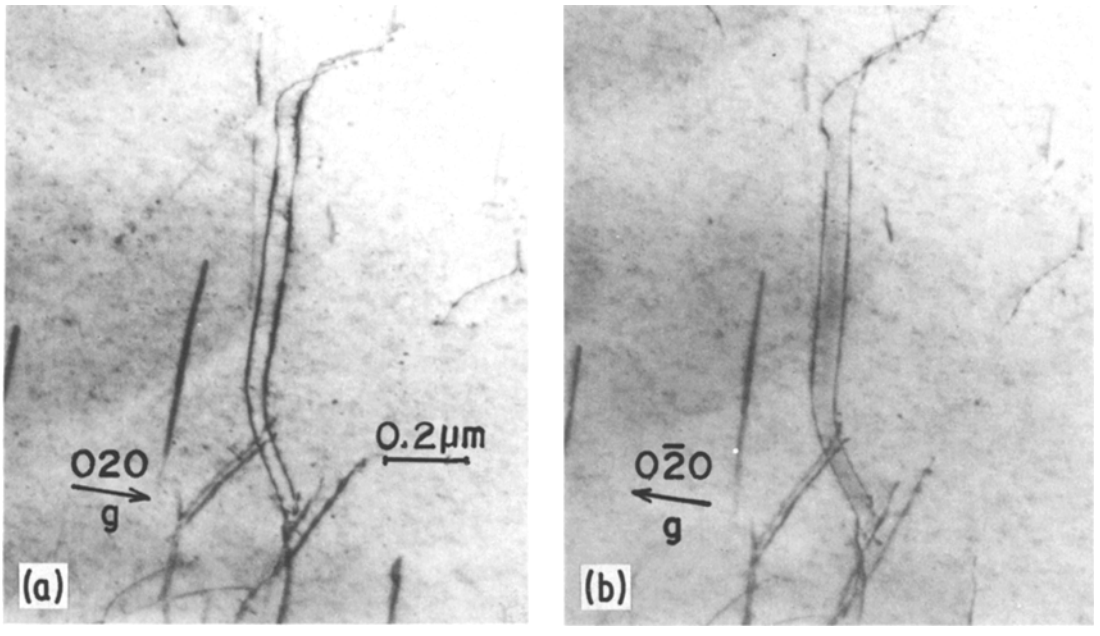

Figure 3 Verification of the dipole formation of edge dislocations by $(\mathbf{g} \cdot \boldsymbol{b})s$ criterion. Note the substantial variation of the spacing by reversing the sign of **g**, keeping s positive.

much higher than for MgO or LiF [8]. The origin of the high work hardening rate is investigated by TEM.

3.2.1. Dislocation intersection

As the foil is parallel to the (0 0 1) plane, straight, elongated dislocations on any active slip plane, (1 0 1), ($\bar{1}$ 0 1), (0 1 1) or (0 $\bar{1}$ 1), have always pure edge character, and the dislocations having screw components are inclined within the foil. On the other hand, the dislocations on an inactive slip plane, (1 1 0) or (1 $\bar{1}$ 0), are either inclined with respect to the surface or appear straight depending on their respective edge or screw character. Fig. 2 demonstrates the intersection of primary slip dislocations with inactive dislocations. Fig. 2a reveals the whole set of dislocations under the condition of multiple reflections, whilst, Fig. 2b reveals, using the 2 0 0 reflection, only the inactive dislocations, of which the upper longer one is of pure screw type with $a/2[\bar{1}\,1\,0]$ Burgers vector. Fig. 2c shows, using 2 2 0 reflection, the primary slip dislocations with $a/2[0\,1\,1]$ or $a/2[0\,1\,\bar{1}]$ Burgers vector, of which most are of the pure edge type. The primary dislocations intersect with the inactive dislocation of the pure screw type, but in this case they cannot interact with each other, and form cusps in the crossed dislocation as seen in Fig. 2b. That the cusps are not the products of dislocation interaction is made clear by the fact that the extinction is complete with 2 2 0 reflection (Fig. 2c). The crossed dislocation is thus transformed into a zigzag. The crossing dislocations are trapped by the crossed one, surround it, and finally form dipoles as is seen in Fig. 2c. This is a possible origin of work hardening in the early stage.

3.2.2. Edge dipole formation

Edge dislocations found on the primary slip plane form, in most cases, dipoles or elongated loops. This is verified by the $(\mathbf{g} \cdot \boldsymbol{b})s$ criterion [9] in Fig. 3. Here **g** is the diffraction vector responsible for the image and $\boldsymbol{b}$ is the Burgers vector of the dislocation in question. The spacing between two parallel edge dislocations varies substantially by reversing the sign of **g**, keeping s positive. The criterion is very important in NiO, because there is a possibility that there could be superlattice dislocations, which would form a magnetic stacking fault between the two parallel edge dislocations. After considerable searching, superlattice dislocations could not be found, probably because of the weak magnetic energy of the fault. This will be discussed in a separate paper.

The fact that dipoles are probably formed by the mechanism of double cross slip and trailing [10, 11], is recently illustrated by *in situ* observation of dislocation motion in MgO [12, 13],

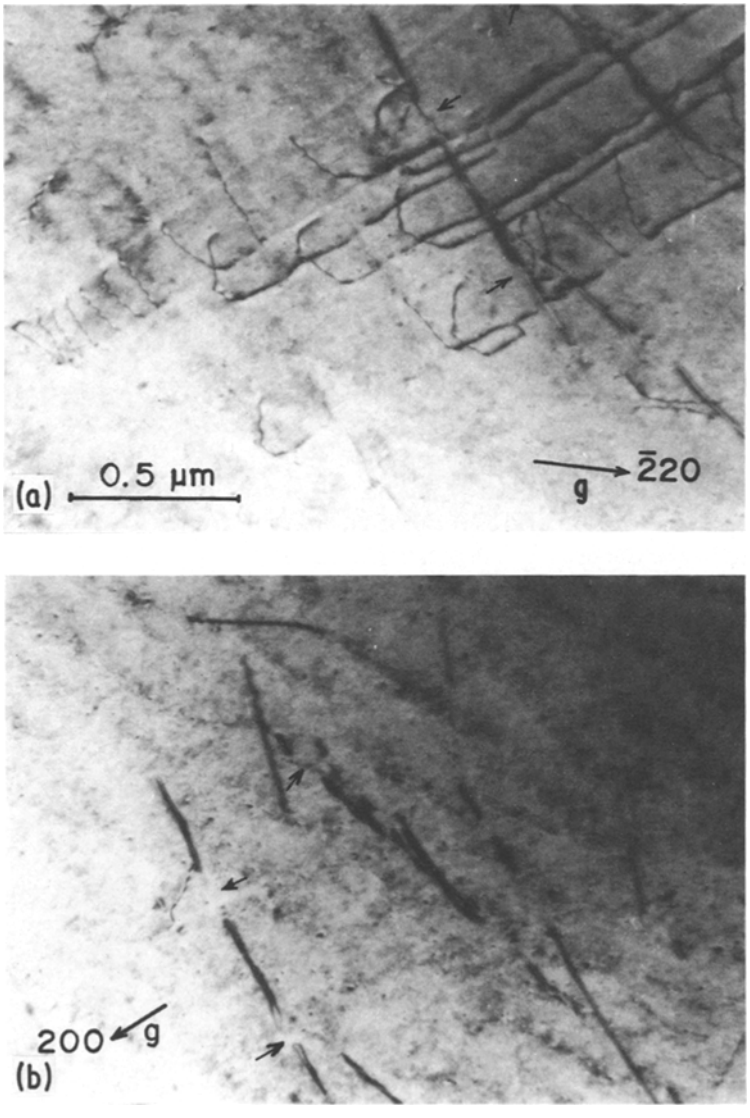

Figure 4 Cut off dislocation dipoles by a series of screw dislocations introduced during manipulation. In (b) only the cut off segments of dipoles are demonstrated. The arrows show the same parts in (a) and (b).

which indicates that there must be strong barriers against dislocations crossing. This is observed in the present experiment in a more or less direct way. A part of the foil was deformed during manipulation, after thinning. The dislocations introduced by this accident are easily distinguished from the existing ones, because the former, which are of a pure screw type and therefore lie in the maximum slope of the slip plane, leave slip traces on the surfaces of the foil, or trail edge components along their slip traces, as shown in Fig. 4a. Where they intersect with the existing edge dipoles, they cut the latter off, and after they have passed through, the edge dipoles shrink to the original position, with the tips rounded in a loop form as in Fig. 4b. This cannot be realized by climb motion, as the thin foil was held at room temperature, but can be done by cross slip on the intersecting (0 1 0) slip plane.

The detailed process is illustrated schematically in Fig. 5. An edge dipole (or elongated dislocation loop) lies on neighbouring $(\bar{1}\,0\,1)$ slip planes. A series of screw dislocations on a (0 1 1) plane introduced during manipulation approaches the dipole, and the leading dislocation intersects with the dipole. The dipole bows on neighbouring $(\bar{1}\,0\,1)$ slip planes, and the pure screw parts of the dipole are annihilated by cross slip on (0 1 0). The cut off segment of the dipole is squeezed out of the foil, which could only be possible in such a case as the stress concentration at the head of dislocation pile up.

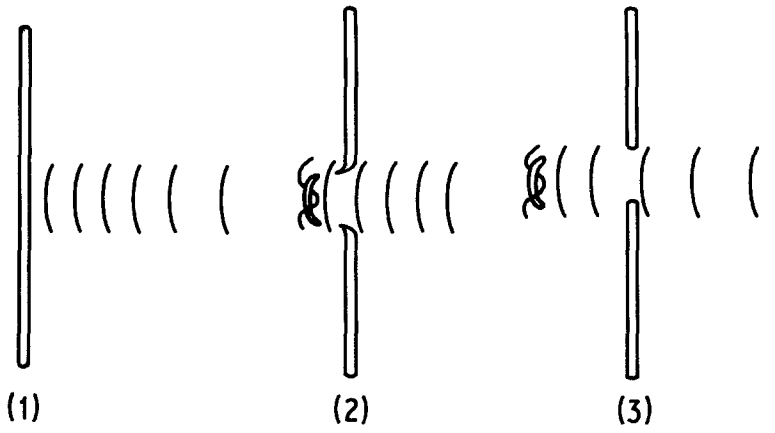

Figure 5 Schematic illustration of the cut off of an edge dipole into segments by a crossing series of dislocations. Projection along [0 0 1] direction.

3.2.3. Dislocation interaction

Dislocation interaction was inspected on the nodes where three dislocations meet. The relation between three Burgers vectors holds in every node. However, in most cases, the reaction is not the result of double slip, but of crystal growth, or of annealing. In fact, the node has the form of a slice of a dislocation network.

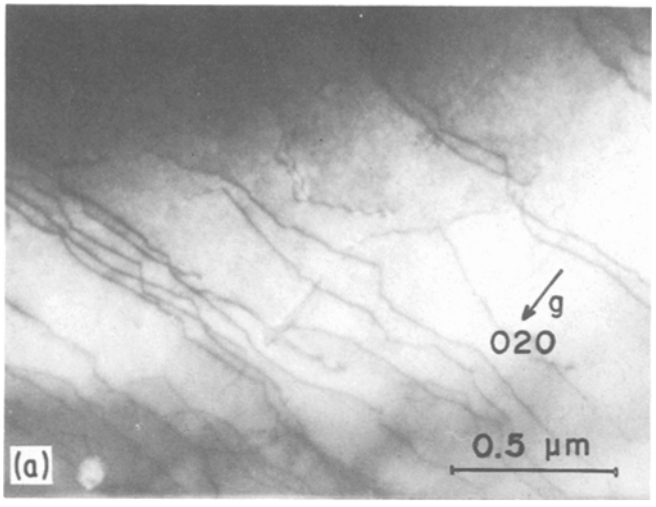

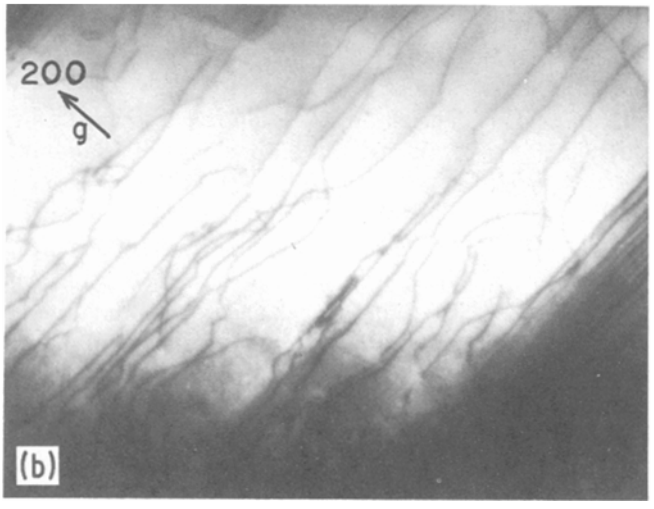

Figure 6 Dislocation interactions as a result of double slip. Note a white hole in lower left, for reference. (a) Primary (crossed) dislocations with $\boldsymbol{b}_1 = a/2[0\,1\,\bar{1}]$. (b) Oblique (crossing) dislocations with $\boldsymbol{b}_2 = a/2[1\,0\,1]$. (c) Whole set of dislocations including resultant dislocations with $\boldsymbol{b}_3 = a/2[1\,1\,0]$. (d) Disappearance of the resultant dislocations. Arrows show the sites of resultant dislocations in (c) and (d).

Fig. 6 (Continued)

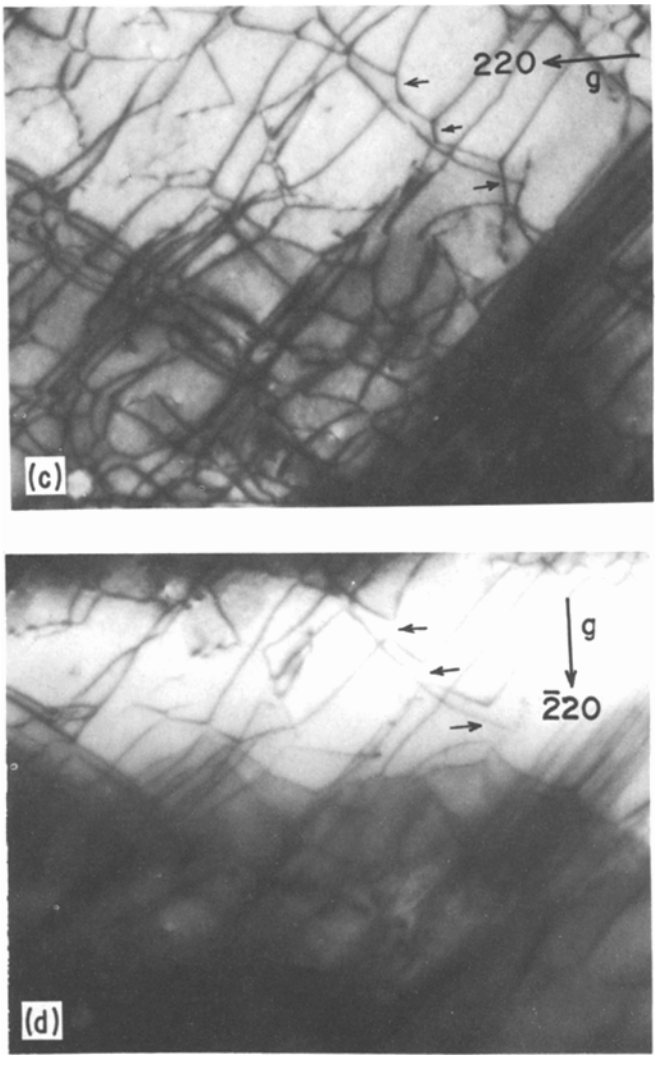

After many efforts, the true interaction of dislocations was found as a result of double slip in a limited region. In Fig. 6a, b and c, primary (crossed), oblique (crossing) and whole dislocations, including the resultant sessile dislocations, are demonstrated using 020, 200 and 220 reflections, because they have Burgers vectors of $\boldsymbol{b}_1 = a/2[0\,1\,\bar{1}]$, $\boldsymbol{b}_2 = a/2[1\,0\,1]$ and $\boldsymbol{b}_3 = a/2[1\,1\,0]$, respectively. The third sessile dislocations disappear in Fig. 6d by the use of $\bar{2}20$ reflection. They lie in this case along the projection of $[1\,\bar{1}\,1]$ direction which is the intersection between primary and secondary (oblique) slip planes. The fact that the third dislocations are produced by the interaction between crossing and crossed dislocations is also identified from the variation in length of those dislocations by intensifying the illumination of electron beam. The dislocation interaction is illustrated schematically in Fig. 7. Primary, oblique and resultant dislocations lying along the $[1\,\bar{1}\,1]$ direction are denoted by 1, 2 and 3, respectively.

It should be noted that the region where the interaction was found had been bent, probably due to glueing with silver paste, as is seen by the extinction contour in the images. Also the density of oblique system dislocations observed in Fig. 6 probably resulted from some local strain concentration, otherwise the strain of the order of 3% would be too small to produce the abundant interaction of dislocations. However it is clear that the interaction will give rise to the intense work hardening characteristic of the secondary stage after several per cent deformation.

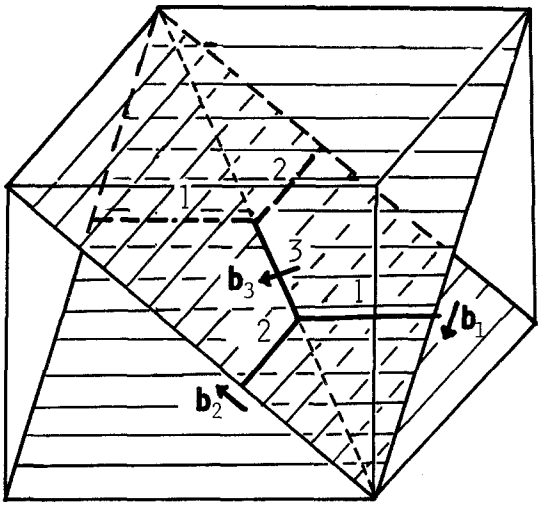

Figure 7 Schematic illustration of the dislocation interaction. Primary, oblique and resultant dislocations are denoted by 1, 2 and 3.

3.2.4. Other sources of work hardening

To find other possible origins of work hardening, for example, dislocation pinning by point imperfections, such as impurity atoms or their precipitates [14], by large jogs [15], by prismatic dislocation loops or by dislocation networks such as small angle grain boundaries, the foils parallel to the active plane would have to be observed.

In-situ observation in a high voltage electron microscope will give more interesting information [16], if we take care about the effect of thickness which has to be at least of the order of 2 to 3 μm [12].

Acknowledgement

The authors thank very much Dr J. Castaing for kindly giving us the specimens, Mr M. Spendel for preparing the foils mechanically, Mr D. Hokim for the ion thinning of them, and Dr J. Castaing and Dr J. P. Rivière for interesting discussions.

References

1. A. DOMINIGUEZ-RODRIGUEZ and J. CASTAING, *C.R. Acad. Sci. Paris* **280** (1975) B317.
2. *Idem, Scripta Metall.* **9** (1975) 551.
3. *Idem, Rev. Phys. Appl.* **11** (1976) 387.
4. A. DOMINIGUEZ-RODRIGUEZ, J. CASTAING and J. PHILIBERT, *Mater. Sci. Eng.* **27** (1977) 217.
5. M. SAURAT and A. REVCOLEVSCHI, *Rev. Int. Hautes Temp. Refract.* **8** (1971) 291.
6. G. W. GROVES and A. KELLY, *Proc. Roy. Soc.* **A275** (1963) 233.
7. J. WASHBURN and Th. CASS, *J. Phys.* **27** (1966) C3-168.
8. M. SRINIVASAN and T. G. STOEBE, *J. Mater. Sci.* **9** (1974) 121.
9. W. BELL, W. R. ROSER and G. THOMAS, *Acta Metall.* **12** (1964) 1247.
10. W. G. JOHNSTON and J. J. GILMAN, *J. Appl. Phys.* **31** (1960) 632.
11. J. WASHBURN, G. W. GROVES, A. KELLY and G. K. WILLIAMSON, *Phil. Mag.* **5** (1960) 991.
12. F. APPEL, H. BETHGE and U. MESSERSCHMIDT, *Phys. Stat. Sol. (a)* **38** (1976) 103.
13. *Idem, ibid.* **42** (1977) 61.
14. H. STRUNK, *Mater. Sci. Eng.* **26** (1976) 231.
15. *Idem, ibid.* **27** (1977) 225.
16. J. CADOZ, D. HOKIM, J. PELISSIER and R. VALLE, *J. Mater. Sci.* **17** (1982) 211.

Received 27 November 1981
and accepted 18 January 1982